RSC Advances

Facile Synthesis and High Formaldehyde-sensing Performance of NiO-SnO2 Hybrid Nanospheres

SCHOLARONE™
Manuscripts

Please do not adjust margins

Journal Name

ARTICLE

Facile Synthesis and High Formaldehyde-sensing Performance of NiO-SnO$_2$ Hybrid Nanospheres

Guochen Zhang,[a] Xue Han,[a] Weiwei Bian[b] Jinhua Zhan,[a] and Xicheng Ma *[a]

A formaldehyde gas sensor with high sensitivity and superior selectivity has been fabricated successfully with NiO-SnO$_2$ hybrid nanospheres, which consisted of n-type porous SnO$_2$ nanospheres and p-type NiO dopants. It has been characterized by X-ray diffraction (XRD), high-resolution electron microscopy (HRTEM), Scanning Electron Microscopy (SEM), X-ray photoelectron spectroscopy (XPS), Brunauer-Emmett-Teller (BET) and energy-dispersive X-ray spectroscopy (EDS). Compared with pure SnO$_2$, the NiO-doped SnO$_2$ nanospheres sensor exhibited significantly enhanced formaldehyde-sensing performances, including lower optimum sensing temperature (about 100°C), lower detectable threshold (0.5ppm), higher sensitivity (Response=26.03 to 50 ppm HCHO) and superior selectivity. Based on our experimental results, the role of the addition of NiO and a possible sensing mechanism has also been discussed.

1 Introduction

Nowadays, people spend typically 80-90% of their time indoors, so that the monitoring of pernicious, toxic and hazardous indoor vapor which is pivotal to keeping our environment clean has been brought to the forefront [1]. Those hazardous indoor vapor such as volatile organic compounds (VOC) generated from indoor decoration not only pollute the environment but also cause various diseases, such as bronchial asthma, atopic dermatitis and sick building syndrome [2]. Formaldehyde (HCHO), as one of the common VOCs, derived mainly from building material, furniture, artificial floor and coating, exhibits a great damage on health such as irritating human eyes and nose, and leading to cancer [3, 4]. The majority of authoritative reviews of the formaldehyde literatures have concluded that an air concentration of 0.3 ppm will provide protection from eye irritation for virtually everyone, and a weight of evidence-based formaldehyde exposure limit of 0.1 ppm is recommended as an indoor air level for all individuals for odor detection and sensory irritation [4]. Many traditional methods to detect HCHO are based on gas chromatographs, mass spectroscopy, FTIR analysis and so on. However, these methods are often costly, time-consuming, and not convenient for wide application [5, 6]. Therefore, developing a simple and portable formaldehyde sensor is extremely urgent.

Tin dioxide (SnO$_2$), a typical n-type semiconductor with a wide band gap of 3.6 eV [7, 8], has been widely used in catalysts [9], lithium ion batteries [10], and transparent electrode [11]. In particular, predominant sensitivity to variations in gaseous environments and excellent chemical stability have made SnO$_2$ become the best known gas-sensing material [12]. However, many problems concerning its working temperature, sensitivity and selectivity remain to be solved. In order to achieve these goals, researchers are focusing on synthesis SnO$_2$ with various morphologies and SnO$_2$-based solid-state gas sensors through modifying the sensing material itself and the fabrication technique [13-15]. Jing et al. electrospun NiO-SnO$_2$ nanofibers which is very selective toward HCHO at 200°C [16]. Wang et al. synthesized SnO$_2$ nanosphere functionalized TiO$_2$ nanobelts which has high response toward HCHO at 300°C [17]. Li et al. in our group synthesized porous SnO$_2$ nanospheres, which also exhibited high sensitivity to HCHO. However, their selectivity and optimum working temperature were not satisfied [18]. As for a portable formaldehyde-sensing device, it is necessary to reduce optimum sensing temperature and enhance selectivity. It has been widely accepted that doping is one of the best ways to enhance selectivity and reduce sensing temperature of a gas sensor. NiO as an effective dopant has received great attention due to its superior sensitivity to toluene and formaldehyde [19, 20].

In this report, a formaldehyde gas sensor based on multi-hierarchy hybrid composite was simply fabricated by modifying SnO$_2$ porous nanospheres with NiO dopants. This hybrid composite provided an indoor air monitoring sensor to achieve ultraselective, sensitive, and reliable detection towards formaldehyde. Compared with pure SnO$_2$ nanospheres, the merged oxides exhibit superior sensing properties at 100°C, opening up an additional avenue to further manipulate individual oxides of interest for gas sensors on demand.

2 Experimental

a. School of Chemistry and Chemical Engineering, Shandong University, Jinan 250100, PR China. E-mail: maxch@sdu.edu.cn; Tel: +86 531 88392430
b. Medical Chemistry Staff Room, Weifang Medical University, Weifang 261053, Shandong, PR China.

2.1 Synthesis of SnO$_2$ nanospheres and NiO-doped SnO$_2$ nanospheres

Tin dichloride (SnCl$_2$•2H$_2$O, ≥98.0%), sodium hypochlorite (NaClO), were purchased from Aladdin Reagent Co. Ltd. Hydrochloric (HCl, 36%), Nickel acetate tetrahydrate (C$_4$H$_6$NiO$_4$•4H$_2$O, 98%) were obtained from Shanghai Chemical Reagent Company and used as received.

The SnO$_2$ porous nanospheres were synthesized similar to our previous work [18]. In a typical procedure, 0.6 mL of HCl and 2.0 mmol of SnCl$_2$•2H$_2$O were dissolved in 30 mL anhydrous ethanol under continuous magnetic stirring. Then 2.0 mmol of NaClO was added into the ethanol solution. After several minutes of stirring, the obtained white slurry was transferred into Teflon-lined steel autoclave. And then it was heated for 24 h at 180°C in an electric oven. After the autoclave was cooled to room temperature, the products were collected and thoroughly washed with distilled water and absolute ethanol.

To obtain NiO-doped SnO$_2$ nanospheres, the product was further dispersed into 5 mL of 0.1 M Ni(CH$_3$COO)$_2$•4H$_2$O ethanol solution followed by ultrasonication for 30 min and centrifugalization at 4000 rpm for 3 min. The product was then dried in a vacuum oven at 60°C for 5 h to remove ethanol and calcinated in air at 400°C for 1 h. After the furnace was cooled to room temperature, the yellow product of NiO-doped SnO$_2$ nanospheres was obtained.

2.2 Characterization and gas sensing measurement

The crystal structure of the product was characterized by X-ray diffraction (XRD Bruker D8). The morphology and microstructure were observed by high-resolution transmission electron microscopy (HRTEM, Japan, JEM-2100, operated at 200 kV) and Scanning Electron Microscopy (SEM, Japan JSM-7600F operated at 5 kV). The elemental analysis were investigated by energy-dispersive X-ray spectroscopy (EDS) using an X-ray micro-analyzer embedded in the JEM-2100 microscope and inductively coupled plasma atomic emission spectroscopy (ICP-AES) on an IRIS Intrepid II XSP instrument. The chemical state of each sample was examined by X-ray photoelectron spectroscopy (XPS, ESCALAB 250, AI Kα). The Brunauer-Emmett-Teller (BET) specific surface areas (SBET) were calculated using the BET equation. Desorption isotherm was used to determine the pore size distribution using the Barret-Joyner-Halender (BJH) method.

To fabricate a gas sensor, the NiO-doped SnO$_2$ powder was mixed in ethanol to produce paste, which was subsequently screen printed onto an alumina tube. This tube was dried at 100°C for 2 h and calcinated at 400°C for 1 h. A Ni–Cr heating wire was then placed inside the tube, which was further aged at 450°C for 120 h to improve the stability and repeatability. Gas sensing properties were measured using a static system controlled by a computer (HW-30A, Hanwei Electronics Co. Ltd.). The operating temperature could be adjusted precisely through the current flow across the Ni–Cr heater. Sensor response (S) was defined as S=Ra/Rg, where the Ra and Rg were resistance in dry air and target gas, respectively.

3 Results and discussion

3.1 Materials preparation and microstructure characterization

Actually, the NiO-doped SnO$_2$ nanospheres were prepared by a three-step procedure in our experiments. The SnO$_2$ porous nanospheres were firstly formed via the hydrothermal process. Secondly, Ni(CH$_3$COO)$_2$•4H$_2$O were doped into the nanopores of the as-formed SnO$_2$ porous nanospheres after ultrasonication in Ni(CH$_3$COO)$_2$•4H$_2$O ethanol solution and dried in a vacuum oven to remove ethanol. Finally, the NiO nuclei were doped into the nanopores of the as-formed SnO$_2$ nanospheres to obtain the NiO-doped SnO$_2$ nanospheres via the decomposition of Ni(CH$_3$COO)$_2$•4H$_2$O to NiO after calcination.

XRD is used to examine the crystal structure of pure SnO$_2$ nanospheres and NiO-doped SnO$_2$ nanospheres. Fig. 1 shows all the strong diffraction peaks which can be perfectly indexed as the tetragonal rutile structure for SnO$_2$ (JCPDS 41-1445, a$_o$=4.738 Å, c$_o$=3.187 Å). Compared with the pure SnO$_2$, there were no evident secondary phases in any of the NiO-doped SnO$_2$ nanospheres. This absence of Ni-related peaks can be due to either the low crystallinity nature of the NiO dopants or the presences of the NiO dopants being simply below the detection limit of X-ray diffraction. This result is similar to our previous work[21].
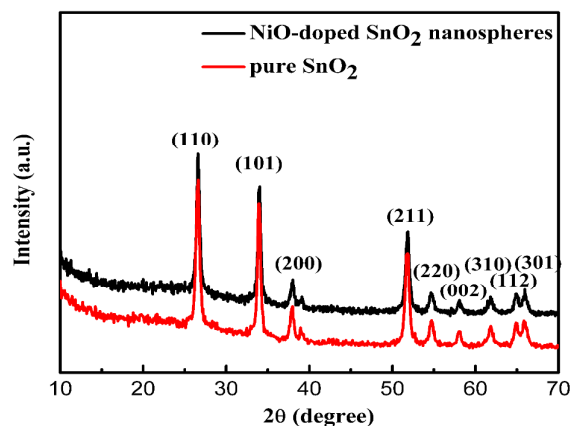

Fig. 1 XRD patterns of pure SnO$_2$ nanospheres (red) and NiO-doped SnO$_2$ nanospheres (black).

The TEM images (Fig. 2a and b) and SEM images (Fig. S1) show the synthesized pure SnO$_2$ and NiO-doped SnO$_2$ nanospheres, respectively. Both of them are highly dominated by the uniform nanospheres with diameters of about 100-200 nm. No obvious differences can be found in the HRTEM images, indicating doping NiO does not obviously change the morphology of SnO$_2$ nanosphere. Each nanosphere is composed of numerous primary nanocrystallites with an average size of about 6 nm and there are plenty of small pores between these interconnected nanocrystallites that confirm their porous nature. Electron diffraction (ED) patterns were also observed, revealing the polycrystalline nature of the two samples. But there is no obvious difference between the two samples due to the low content or poor crystallinity nature of these NiO dopants. Further EDS analysis of the products, as shown in Fig. 2 (c and d), point out that the Ni chemical elements consist in the NiO-doped SnO$_2$ nanospheres, while the pure SnO$_2$ nanospheres are composed of only two elements: Sn and O, proving Ni chemical elements were successfully

doped into the pure SnO$_2$ nanospheres. The appearance of copper signals is attributed to the supporting TEM wire gauze in measurement. On the basis of the results of the EDS analysis, the average atomic ratio of Ni/Sn in these nanospheres is estimated to be about 1:30. It should be further mentioned that the EDS analysis taken from different nanospheres of the products showed only a little difference in values. This may be an indication of the homogeneity of the prepared materials in the micro-scale level. A further ICP technique was also used to measure the chemistry composition of the as-formed NiO-doped SnO$_2$ nanospheres, the obtained atomic ratio of Ni to Sn is 1:27, which is very close to that of obtained by using EDS.
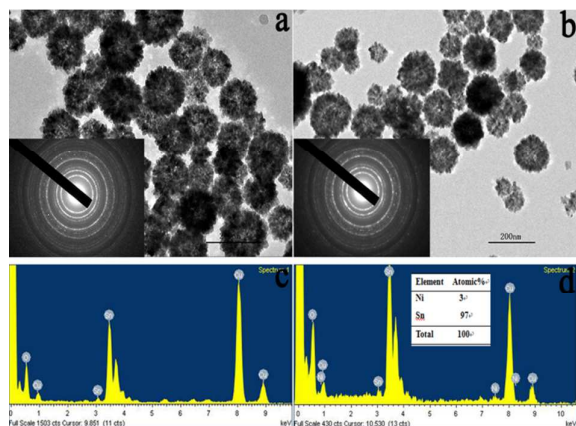

Fig. 2 (a) TEM image and SAED pattern of pure SnO$_2$ nanospheres; (b) TEM image and SAED pattern of NiO-doped SnO$_2$ nanospheres; (c) EDS pattern of pure SnO$_2$ nanospheres; (d) EDS pattern of NiO-doped SnO$_2$ nanospheres.

The specimens were further analyzed using XPS to investigate the physicochemical states of the samples and to confirm the incorporation of NiO into SnO$_2$ nanospheres. Fig. 3a shows the XPS survey spectrum of the NiO-doped SnO$_2$ sample. The peaks for O 1s at 530.1 eV, Sn 3d5/2 at 486.2 eV and Sn 3d3/2 at 494.7 eV are in good agreement with the values for the lattice oxygen and tin of SnO$_2$, respectively [22]. It has been revealed that nickel should have oxidation peaks located at 855.6 and 861.2 eV for NiO [23]. In our experiments, due to the low concentration of Ni in the composite of NiO-doped SnO$_2$ nanospheres, as already revealed by EDS, ICP and XRD, the peaks for Ni 2p are ambiguous for observation. However, when enlarging the view in the range of 850–862 eV (Fig. 3c), some small peaks still can be clearly distinguished, which should be ascribed to Ni in oxidation state on the nanospheres surface.

In Fig. 3b, the binding energy ranges of Sn 3d of both pure SnO$_2$ and NiO-doped SnO$_2$ were plotted together for comparisons. It can be seen from this figure that the Sn 3d binding energy values of NiO-doped SnO$_2$ are lower than that of undoped SnO$_2$. This means that the Fermi level of the NiO-doped SnO$_2$ sample goes down towards the valence band edge, and the O^{2-} ions placed near to the Ni sites possess a higher mobility [16]. The peaks were not symmetric in the high resolution XPS spectrum for oxygen in the hybrid composite. The phenomena implied that there were several chemical states of oxygen exist in the samples. To understand the change of chemical states, the XPSPEAK program (version 4.1) was used to obtain the deconvolution peaks. In Fig. 3d, compared with the undoped SnO$_2$, there is a redundant peak. The peak at 530.5 eV is ascribed to Sn-O-Sn lattice species without oxygen defects [24],

and the features at 530.1 eV are assigned to the oxygen vacancies (V$_o$) in the oxide lattices [25]. The peak at 531.7 eV could be associated with the oxide in hydroxide [26]. It is reasonable that oxygen vacancy and defects could increase the gas response.
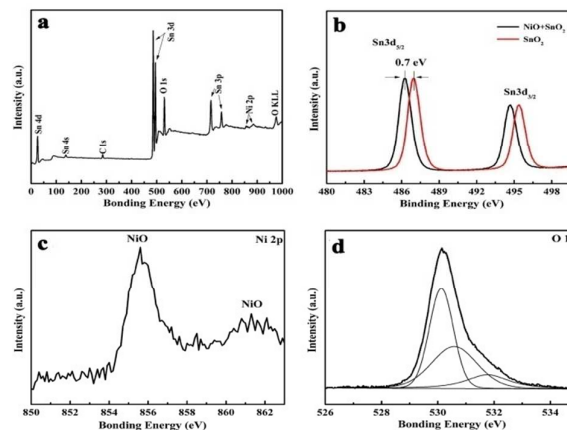

Fig. 3 XPS spectra of the NiO-doped SnO$_2$ nanospheres: (a) survey spectrum; (b) compare spect of Sn 3d (black: NiO-doped SnO$_2$ nanospheres, red: pure SnO$_2$ nanospheres); (c) Ni 2p and (d) O 1s.

3.2 Gas sensing properties

Firstly, the influence of NiO-doping on SnO$_2$ sensor's sensitivity for formaldehyde detecting at different temperature was investigated. A pure SnO$_2$ nanospheres based sensor was also fabricated for comparison. Fig.4 shows the response of the sensors to 50.0 ppm formaldehyde at different operating temperature ranging from 50℃ to 400℃. It can be observed that the responses of the NiO-doped SnO$_2$ nanospheres sensor increased with operating temperature until reached their maximum response 26.03 at 100°C and then decreased rapidly with further raising the operating temperature. However, for the pure SnO$_2$ nanospheres, the maximum response value is only 6.63 at 240℃, which is about 4 times lower than NiO-doped SnO$_2$ nanospheres. These results indicate that the addition of NiO dopants can not only efficiently reduce energy consumption with a lower optimum sensing temperature but also greatly improve the sensitivity of the sensor. At the optimum sensing temperature of 100°C, the lowest HCHO concentration which can be detected by NiO-doped SnO$_2$ nanospheres is 0.5 ppm with a response of 2.40, as shown in Fig S3.

Secondly, in order to further understand their sensing characteristics, the response and recovery transient properties of both the pure SnO$_2$ nanospheres and the NiO-doped SnO$_2$ nanospheres sensors were further comparatively studied in the formaldehyde concentration ranging from 1 to 100 ppm,. Because the pure SnO$_2$ nanospheres show poor response at 100°C, which is the optimum sensing temperature of NiO-doped SnO$_2$ nanospheres, we performed the comparative study at 200°C. The obtained results are shown in Fig. 5. It can be seen that six response cycles were successively recorded, and gas sensors based on both pure SnO$_2$ nanospheres and NiO-doped SnO$_2$ nanospheres show good sensitivity to formaldehyde. However, NiO-doped SnO$_2$ nanospheres show much higher responses value than undoped

SnO_2 nanospheres to any given HCHO concentration. At this sensing temperature (200 ° C), the response of NiO-doped hetero-nanospheres sensor to 100 ppm formaldehyde is 22.30.
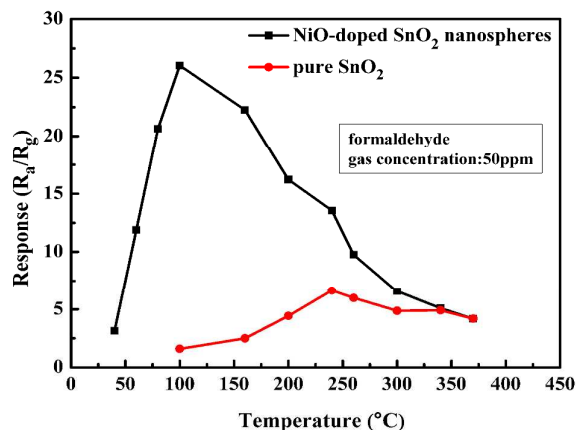

Fig. 4 Gas response versus operating temperature of pure SnO_2 nanospheres (red) and NiO-doped SnO_2 nanospheres (black) to 50 ppm formaldehyde.
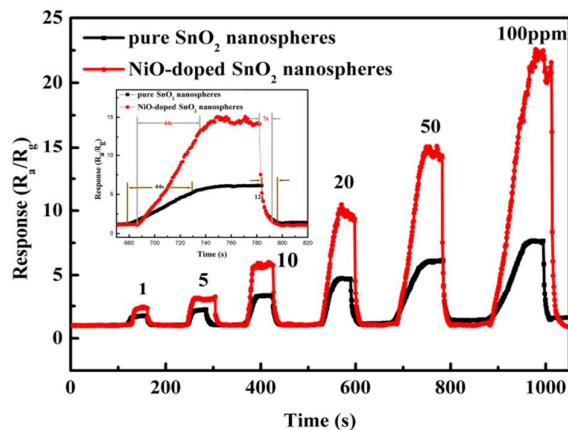

Fig. 5 Dynamic sensing response to formaldehyde gas (1-100 ppm) of pure SnO_2 nanospheres (black) and NiO-doped SnO_2 nanospheres (red); the inset is an image of enlarged drawing at the concentration of 50 ppm.

The response and recovery time of the sensors were also comparatively measured. The response and recovery time are important parameters for gas sensor. The response time is defined as the time required for the response signal to reach 90% of the sample conductance variation after the injection of test gas. The recovery time is defined as the time needed to return to 10% above the original response in air after the test gas has been released [27]. As shown in Fig. 5, the NiO-doped SnO_2 nanospheres based sensor exhibits similar response time but shorter recovery time to formaldehyde compared with pure SnO_2 nanospheres based sensor. The shorter recovery time are almost unchanged at all the tested concentrations of formaldehyde. As an example when exposed to 50.0 ppm formaldehyde, the calculated response and recovery times are about 44 and 7 s for the NiO-doped SnO_2 nanospheres

based sensor, and about 44 and 12 s for pure SnO_2 nanosphere, both at 200°C of sensor operating temperature.

Selectivity is another very important parameter for a utility-type metal oxide gas sensor, because poor selectivity will induce mistaken alarm and limit its extensive utilization [28]. Finally, in order to further investigate the selectivity of both the pure SnO_2 porous nanospheres and the NiO-doped SnO_2 nanospheres, some other typical VOCs gases such as acetone, ethanol, methylbenzene, 2-chlorophenol and chloroform were also tested for comparison, as shown in Fig. 6. All the analyte gases are of the same concentration of 50.0 ppm. The working temperature of the sensor is at 100°C. From Fig. 6, it can be clearly seen that the responses of the sensor based on pure SnO_2 porous nanospheres to all the tested analyte gases are lower than 5 and with poor selectivity. However, the sensor based on NiO-doped SnO_2 nanospheres shows the highest sensitivity to formaldehyde (26.03), which is higher than that of ethanol (4.7) and much higher than that of methylbenzene (1.3), acetone (1.9), chloroform (1.7), and 2-chlorophenol (1.3), implying that the NiO-doped SnO_2 nanospheres are more sensitive to formaldehyde gas and could be a very promising candidate for selectively detecting formaldehyde gas, which further indicates that the selectivity properties of pure SnO_2 nanospheres has been significantly enhanced by the NiO-doping.
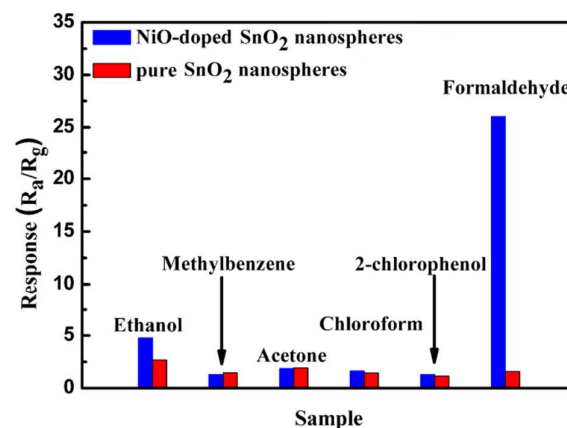

Fig. 6. Gas response of both NiO-doped SnO_2 nanospheres (blue) and pure SnO_2 nsnospheres (red) to various gases including ethanol, acetone, formaldehyde, methylbenzene, 2-chlorophenol and chloroform.

The effect of relative humidity (RH) on the sensor performance was also investigated. Figure 7 shows the gas response of NiO-doped SnO2 nanospheres to 50 ppm formaldehyde at an operating temperature of 100°C in different RH atmospheres. The response (S= $R_{hum-air}/R_{hum-gas}$) of the sensor was defined as the ratio of sensor resistance in humid air ($R_{hum-air}$) to that in humid air with 50 ppm formaldehyde ($R_{hum-gas}$). From this figure, we can see that the sensor performances were influenced by relative humidity. The gas response of the NiO-doped SnO_2 nanospheres increase with the rise of RH, up to a maximum value, then decrease with the rise of RH. The maximum response of sample nanospheres to 50 ppm formaldehyde was about 29.48 at 40% RH. The influence of RH on the sensor performance can be tentatively ascribed to the adsorption competition between the H_2O and formaldehyde molecules on the SnO_2 surface and the enhancement of the

dissociated water to the conduction of SnO_2 surface[29]. A further detailed investigation of the sensor characteristics in humid atmospheres is beyond the scope of this paper, but is now in progress.
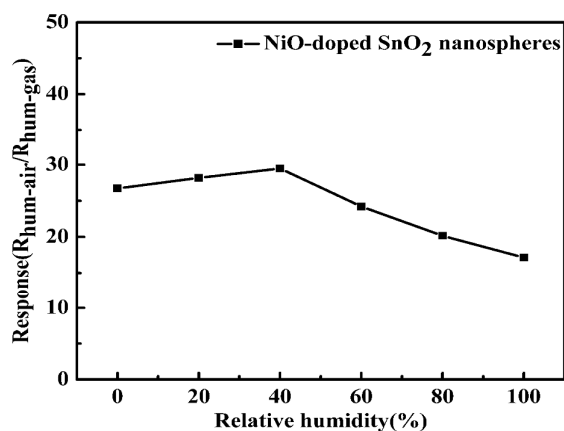

Figure 7 Gas response of NiO-doped SnO$_2$ nanospheres to 50 ppm formaldehyde in different relative humidity at an operating temperature of 100° C. The response is defined as the ratio of sensor resistance in humid air (R$_{hum-air}$) to that in humid air with 50ppm formaldehyde (R$_{hum-gas}$).

Furthermore, the sensitivity reproducibility and long-time stability of the sensors have been measured. For instance, the reproducibility measurement confirms that the sensor based on NiO-doped SnO$_2$ nanospheres maintains its initial response without a clear variation upon five successive sensing measurements to 50 ppm HCHO gas at 100° C (as shown in Fig. 8a). Meanwhile, the sensor exhibits a good stability towards 50 ppm HCHO in 14 days (as shown in Fig. 8b). These findings convincely verify our sensor could possess excellent stability in short and long term, respectively.
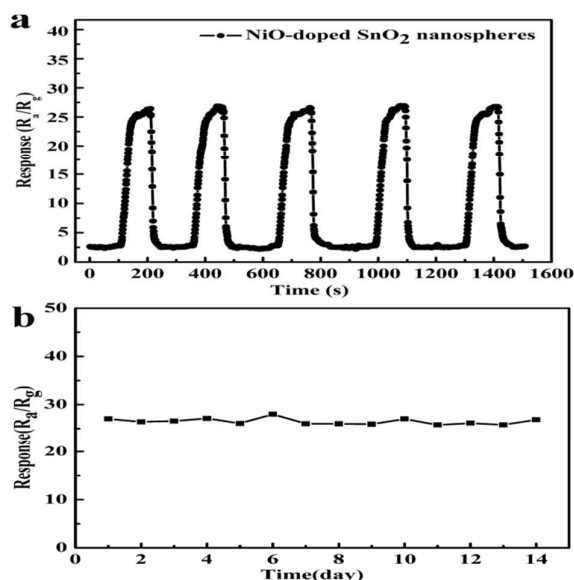

Fig. 8 (a) Sensitivity reproducibility of the NiO-doped SnO$_2$ nanospheres to 50 ppm of formaldehyde at 100°C. (b) Stability of NiO-doped SnO$_2$ nanospheres to 50 ppm formaldehyde at 100° C.

3.3. Gas sensing mechanism

The commonly recognized gas sensing mechanism for SnO$_2$-based sensing materials at high work temperature is mainly described as an adsorption–oxidation–desorption process in which chemisorbed oxygen plays a crucial role [30]. As tin oxide is exposed to ambient air, the surface of SnO$_2$ will adsorb oxygen molecules which could trap electrons from the conduction band of SnO$_2$ to form adsorbed oxygen species (O_2^-, O^-, O^{2-}), and result in an electron-depletion layer at surface. When the sensor is exposed to reductive formaldehyde, the formaldehyde molecules would react with the adsorbed oxygen species, thereby releasing the trapped electrons back into the SnO$_2$ and decreasing the thickness of electron-depletion layer. As a result, the resistance change can be found [31]. Therefore, the amount of chemisorbed oxygen on the surface is critical for the thickness of electron-depletion and the performance of the sensor.

Many previous studies have reported that specific surface area is responsible for an improvement of the response of gas sensing [32, 33]. In our experiments, as calculated by the Brunauer-Emmett-Teller (BET) specific surface area from nitrogen isotherm in Fig.S2, the specific surface area of the pure SnO$_2$ is 39.48 m^2 g^{-1}, which is much larger than that of the NiO-doped SnO$_2$ (27.69 m^2 g^{-1}), while the NiO-doped SnO$_2$ shows a better gas-sensing response. To make clear such a phenomenon, electrical resistances of both the pure SnO$_2$ and NiO-doped SnO$_2$ sensors in air (Ra) as a function of temperatures (40-400°C) were measured. (Fig. S4). The addition of NiO dopants results in an extensive increase in the value of Ra especially when the temperatures below 200°C. For example, the electrical resistance in air of the NiO-doped SnO$_2$ sensor increases by almost four times as compared with that of the pure SnO$_2$ sensor at 100°C. This kind of resistance increasing due to doping has also been widely observed in the cases of NiO–In$_2$O$_3$ and NiO–SnO$_2$ [34-36]. We believe that this effect is the first possible reason caused the sensing enhancement of NiO-doped SnO$_2$ sensor.

It is well-known that the surface of SnO$_2$ nanospheres only chemisorbed a half-baked monolayer of oxygen, but when the Ni was doped in the SnO$_2$ nanospheres, the Ni ions can easy aggregate a full monolayer of oxygen ions which can be oxidized into a higher oxidation state [37, 38]. Furthermore, NiO is one of the most promising materials used for the oxidation of HCHO, which could be used for formaldehyde sensing individually [39, 40]. When the NiO-doped SnO$_2$ nanospheres sensor is exposed to HCHO gas, the HCHO molecules will be adsorbed and react with oxygen ions in higher oxidation state on the surface of NiO. This is probably the second reason that caused the significant enhancement of sensitivity and selectivity towards HCHO at 100°C by NiO-doping.

Moreover, the sensing enhancement of NiO-doped SnO$_2$ could also be accounted for the formation of P-N junction by adding the NiO. It is well-known that SnO$_2$ mainly shows n-type conductivity by electrons and NiO displays p-type conductivity by holes. Compared with pure SnO$_2$ sensor, the sensing mechanism will be different after the formation of P–N heterostructure [41]. As shown in Fig. 9a, in order to fit the equalization of the Fermi levels, the contact between n-type SnO$_2$ and p-type NiO results in band bending in the depletion layers on either side of the physical interface. When the heterostructure sensor is working at high temperature in air, besides the depletion layer formed on the surface of SnO$_2$

nanospheres, the depletion region at the heterostructure interface will lead to the resistance of the NiO-doped SnO_2 nanosphere in air (Ra) being higher than the pure SnO_2 nanospheres, as already confirmed in our experiments as Fig S4. Once exposed to formaldehyde gas, the formaldehyde molecules will react with oxygen species, releasing the electrons back to the conduction band and causing the resistance to decrease. In addition, electrons released from formaldehyde combine with holes in p-type NiO, leading to the reduction of concentration gradient on both sides of P–N junction. Both of these effects decrease the resistance of NiO-doped SnO_2 sensor, as shown in Fig. 9b. In summary, the formation of P–N junction enormously increases the resistance of SnO_2 sensor in air and further decreases the resistance in formaldehyde gas, which hence leads to NiO-doped SnO_2 sensor with high sensitivity and great selectivity towards formaldehyde.
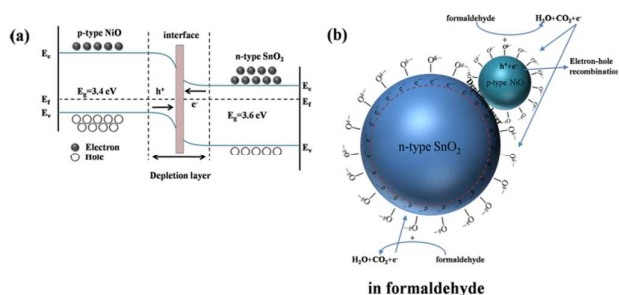

Fig. 9 (a) Proposed ideal band structure for a p-NiO/n-SnO$_2$ heterostructure. Ec: lower level of conduction band; Ef: Fermi level; Ev: upper level of valence band. (b) schematic model for the p-type NiO/n-type SnO$_2$ heterostructure based sensor when exposed to formaldehyde gas.

Conclusions

In conclusion, NiO-doped SnO_2 nanospheres hybrid composite have been fabricated via facile impregnation technique and calcination process. The sensor exhibited greatly enhanced formaldehyde sensing properties compared with the pure SnO_2 nanospheres, including lower operating temperature, higher sensitivity, lower detectable threshold and superior selectivity. The enhanced sensing properties to formaldehyde are mainly attributed to the addition of NiO and the formation of SnO_2/NiO heterostructure. This work shed some new light on design and fabrication of the complex nanostructures gas sensors with high sensing performances.
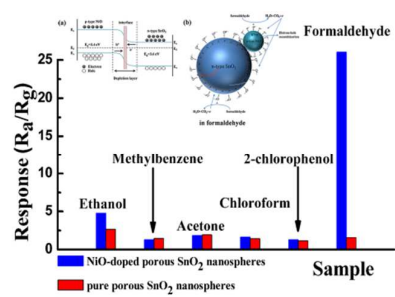
Acknowledgements

Notes and references

1   G. Ingrosso, Free radical chemistry and its concern with indoor air quality: an open problem, Microchemical Journal, 73 (2002) 221-236.

2   K. Kawamura, K. Kerman, M. Fujihara, N. Nagatani, T. Hashiba, E. Tamiya, Development of a novel hand-held formaldehyde gas sensor for the rapid detection of sick building syndrome, Sensors and Actuators B: Chemical, 105 (2005) 495-501.

3   Y. Herschkovitz, I. Eshkenazi, C.E. Campbell, J. Rishpon, An electrochemical biosensor for formaldehyde, Journal of Electroanalytical Chemistry, 491 (2000) 182-187.

4   R. Golden, Identifying an indoor air exposure limit for formaldehyde considering both irritation and cancer hazards, Critical Reviews in Toxicology, 41 (2011) 672-721.

5   M. C. Hunter, K. D. Bartle, P. W. Seakins, A. C. Lewis, Direct measurement of atmospheric formaldehyde using gas chromatography-pulsed discharge ionisation detection, Analytical Communications, 36 (1999) 101-104.

6   S. Kim, H.-J. Kim, Comparison of standard methods and gas chromatography method in determination of formaldehyde emission from MDF bonded with formaldehyde-based resins, Bioresource Technology, 96 (2005) 1457-1464.

7   B. Cheng, J.M. Russell, Shi, L. Zhang, E.T. Samulski, Large-Scale, Solution-Phase Growth of Single-Crystalline SnO2 Nanorods, Journal of the American Chemical Society, 126 (2004) 5972-5973.

8   D.F. Zhang, L.D. Sun, J.L. Yin, C.H. Yan, Low-Temperature Fabrication of Highly Crystalline SnO2 Nanorods, Advanced Materials, 15 (2003) 1022-1025.

9   G. Wang, W. Lu, J. Li, J. Choi, Y. Jeong, S.-Y. Choi, J.-B. Park, M.K. Ryu, K. Lee, V-Shaped Tin Oxide Nanostructures Featuring a Broad Photocurrent Signal: An Effective Visible-Light-Driven Photocatalyst, Small, 2 (2006) 1436-1439.

10 W.-S. Kim, Y. Hwa, J.-H. Jeun, H.-J. Sohn, S.-H. Hong, Synthesis of SnO2 nano hollow spheres and their size effects in lithium ion battery anode application, Journal of Power Sources, 225 (2013) 108-112.

11 G. Giusti, V. Consonni, E. Puyoo, D. Bellet, High Performance ZnO-SnO2:F Nanocomposite Transparent Electrodes for Energy Applications, ACS Applied Materials & Interfaces, 6 (2014) 14096-14107.

12 N.M. Shaalan, T. Yamazaki, T. Kikuta, Synthesis of metal and metal oxide nanostructures and their application for gas sensing, Materials Chemistry and Physics, 127 (2011) 143-150.

13 F. Gyger, M. Hübner, C. Feldmann, N. Barsan, U. Weimar, Nanoscale SnO2 Hollow Spheres and Their Application as a Gas-Sensing Material, Chemistry of Materials, 22 (2010) 4821-4827.

14 K.-M. Kim, K.-I. Choi, H.-M. Jeong, H.-J. Kim, H.-R. Kim, J.-H. Lee, Highly sensitive and selective trimethylamine sensors using Ru-doped SnO2 hollow spheres, Sensors and Actuators B: Chemical, 166–167 (2012) 733-738.

15 Q. Lin, Y. Li, M. Yang, Tin oxide/graphene composite fabricated via a hydrothermal method for gas sensors working at room temperature, Sensors and Actuators B: Chemical, 173 (2012) 139-147.

16 Y. Zheng, J. Wang, P. Yao, Formaldehyde sensing properties of electrospun NiO-doped SnO2 nanofibers, Sensors and Actuators B: Chemical, 156 (2011) 723-730.

17 W. Zeng, T. Liu, Z. Wang, Enhanced gas sensing properties by SnO2 nanosphere functionalized TiO2 nanobelts, Journal of Materials Chemistry, 22 (2012) 3544-3548.

18 Z. Li, Q. Zhao, W. Fan, J. Zhan, Porous SnO2 nanospheres as sensitive gas sensors for volatile organic compounds detection, Nanoscale, 3 (2011) 1646-1652.

19 X. Lai, G. Shen, P. Xue, B. Yan, H. Wang, P. Li, W. Xia, J. Fang, Ordered mesoporous NiO with thin pore walls and its enhanced sensing performance for formaldehyde, Nanoscale, 7 (2015) 4005-4012.

20 H.-J. Kim, J.-W. Yoon, K.-I. Choi, H.W. Jang, A. Umar, J.-H. Lee, Ultraselective and sensitive detection of xylene and toluene for monitoring indoor air pollution using Cr-doped NiO hierarchical nanostructures, Nanoscale, 5 (2013) 7066-7073.

21 X. Ma, H. Song, C. Guan, Enhanced ethanol sensing properties of ZnO-doped porous SnO2 hollow nanospheres, Sensors and Actuators B: Chemical, 188 (2013) 193-199.

22 T.L. Barr, An ESCA study of the termination of the passivation of elemental metals, The Journal of Physical Chemistry, 82 (1978) 1801-1810.

23 K.S. Kim, R.E. Davis, Electron spectroscopy of the nickel-oxygen system, Journal of Electron Spectroscopy and Related Phenomena, 1 (1972) 251-258.

24 B.F. Dzhurinskii, D. Gati, N.P. Sergushin, V.I. Nefedov, Y.V. Salyn, Simple and coordination compounds. An X-ray photoelectron spectroscopic study of certain oxides, Russian Journal of Inorganic Chemistry, 20 (1975) 2307-2314.

25 D.-J. Yang, I. Kamienchick, D.Y. Youn, A. Rothschild, I.-D. Kim, Ultrasensitive and Highly Selective Gas Sensors Based on Electrospun SnO2 Nanofibers Modified by Pd Loading, Advanced Functional Materials, 20 (2010) 4258-4264.

26 I. Olefjord, B. Brox, U. Jelvestam, Surface composition of stainless steels during anodic dissolution and passivation studied by ESCA, Journal of the Electrochemical Society, 132 (1985) 2854-2861.

27 J. Liu, X. Wang, Q. Peng, Y. Li, Vanadium Pentoxide Nanobelts: Highly Selective and Stable Ethanol Sensor Materials, Advanced Materials, 17 (2005) 764-767.

28 M. Bagheri, N.F. Hamedani, A.R. Mahjoub, A.A. Khodadadi, Y. Mortazavi, Highly sensitive and selective ethanol sensor based on Sm2O3-loaded flower-like ZnO nanostructure, Sensors and Actuators B: Chemical, 191 (2014) 283-290.

29 M. Li, L.J. Qiao, W.Y. Chu, A.A. Volinsky, Water pre-adsorption effect on room temperature SnO2 nanobelt ethanol sensitivity in oxygen-deficient conditions, Sensors and Actuators B: Chemical, 158 (2011) 340-344.

30 G. Korotcenkov, Metal oxides for solid-state gas sensors: What determines our choice?, Materials Science and Engineering: B, 139 (2007) 1-23.

31 A. Gurlo, R. Riedel, In situ and operando spectroscopy for assessing mechanisms of gas sensing, Angewandte Chemie International Edition, 46 (2007) 3826-3848.

32 L. Wang, T. Fei, Z. Lou, T. Zhang, Three-dimensional hierarchical flowerlike α-Fe2O3 nanostructures: synthesis and

ethanol-sensing properties, ACS applied materials & interfaces, 3 (2011) 4689-4694.

33 L. Wang, X. Luo, X. Zheng, R. Wang, T. Zhang, Direct annealing of electrospun synthesized high-performance porous SnO 2 hollow nanofibers for gas sensors, RSC Advances, 3 (2013) 9723-9728.

34 M. Ivanovskaya, P. Bogdanov, G. Faglia, G. Sberveglieri, The features of thin film and ceramic sensors at the detection of CO and NO 2, Sensors and Actuators B: Chemical, 68 (2000) 344-350.

35 M. Ivanovskaya, P. Bogdanov, Effect of Ni II ions on the properties of In 2 O 3-based ceramic sensors, Sensors and Actuators B: Chemical, 53 (1998) 44-53.

36 P. Bogdanov, M. Ivanovskaya, E. Comini, G. Faglia, G. Sberveglieri, Effect of nickel ions on sensitivity of In 2 O 3 thin film sensors to NO 2, Sensors and Actuators B: Chemical, 57 (1999) 153-158.

37 M. Calatayud, A. Markovits, M. Menetrey, B. Mguig, C. Minot, Adsorption on perfect and reduced surfaces of metal oxides, Catalysis Today, 85 (2003) 125-143.

38 V.E. Henrich, The surfaces of metal oxides, Reports on Progress in Physics, 48 (1985) 1481.

39 G. Li, X. Wang, H. Ding, T. Zhang, A facile synthesis method for Ni (OH) 2 ultrathin nanosheets and their conversion to porous NiO nanosheets used for formaldehyde sensing, RSC Advances, 2 (2012) 13018-13023.

40 J.A. Dirksen, K. Duval, T.A. Ring, NiO thin-film formaldehyde gas sensor, Sensors and Actuators B: Chemical, 80 (2001) 106-115.

41 D.R. Miller, S.A. Akbar, P.A. Morris, Nanoscale metal oxide-based heterojunctions for gas sensing: A review, Sensors and Actuators B: Chemical, 204 (2014) 250-272.

Graphical abstract

"Facile Synthesis and High Formaldehyde-sensing Performance of NiO-SnO$_2$ Hybrid Nanospheres"

A formaldehyde gas sensor with high sensitivity and superior selectivity has been fabricated successfully with NiO-SnO$_2$ hybrid nanospheres.